Master's thesis

NTNU
Norwegian University of Science and Technology
Faculty of Natural Sciences
Department of Physics

Preben Gjelsvik

Optical Properties of Intermediate Band Ca_6FeN_5 and Related Materials: A Density Functional Theory Study

Master's thesis in MSPHYS
Supervisor: Jon Andreas Støvneng
June 2023

NTNU
Norwegian University of
Science and Technology

Preben Gjelsvik

Optical Properties of Intermediate Band Ca_6FeN_5 and Related Materials: A Density Functional Theory Study

Master's thesis in MSPHYS
Supervisor: Jon Andreas Støvneng
June 2023

Norwegian University of Science and Technology
Faculty of Natural Sciences
Department of Physics

NTNU
Norwegian University of
Science and Technology

NTNU
Kunnskap for en bedre verden

Department of Physics

FY3900 - Master Thesis in Physics

Optical Properties of Intermediate Band Ca_6FeN_5 and Related Materials: A Density Functional Theory Study

Author:
Preben Gjelsvik

Supervisor:
Jon Andreas Støvneng

15th of June, 2023

Abstract

This thesis describes and demonstrates a method for identifying new intermediate band materials for solar cell applications using Density Functional Theory. Ca_6FeN_5 and variants of it constructed by substituting Ca and N with Mg and P respectively have been studied to see how the substitutions affect the electronic band structure. The results show that such substitutions can have a significant effect on the electronic band structure, including increasing or decreasing the size of the band gaps.

Sammendrag

Denne oppgaven beskriver og demonstrerer en metode for å identifisere nye mellombåndsmaterialer for solceller ved å bruke tetthetsfunksjonalteori. Ca_6FeN_5 og varianter konstruert ved å erstatte Ca og N med henholdsvis Mg og P har blitt studert for å se hvordan substitusjonene påvirker den elektroniske båndstrukturen. Resultatene viser at slike erstatninger kan ha en betydelig effekt på den elektroniske båndstrukturen, inklusivt å øke eller redusere størrelsen på båndgapene.

Preface

This is my master's thesis in physics at the Norwegian University of Science and Technology (NTNU). It marks the end of a six-year long journey of studying physics at NTNU where I've learned a lot about physics and mathematics, but also chemistry, IT, and most importantly, a lot about myself.

I want to give a special thanks to my supervisor Jon Andreas Støvneng for all the great support, even when things were difficult, and for many entertaining and instructive conversations.

I also want to give a special thanks to Ståle Reklev whom I've studied with all these years for being a great friend and study partner, especially for motivating me to keep going even when I wanted to give up studying.

I would also like to thank Turid Reenaas for help with finding the topic for my thesis, as well as relevant articles to read.

Lastly, I want to thank my family and all other friends for all the love and support, and my former teachers for helping me get to this point in the first place.

Table of Contents

1 Introduction

Increased efficiency of solar cells can be an important part of holding back climate change, especially if new types of solar cells using more sustainable materials can be found. Intermediate band solar cells are a type of solar cell that can overcome the Shockley–Queisser limit by introducing an intermediate band situated between the valence band and the conduction band [8]. Because of this, identifying materials that have an intermediate band with desirable properties is of special interest. Baquião and Dalpian [2] performed a computational screening using AFLOW [1] that resulted in three potential candidates worth taking a closer look at. One of those materials, Ca_6FeN_5, will be used as the basis for this study.

The goal of this study is to look at the possibility of finding more intermediate band candidates or candidates with better properties by making modifications to known structures. One relatively gentle way to modify a material is to replace one or more atoms in the unit cell with other atoms from the same group. Although doing partial substitutions would be of interest as well, the scope of this study is limited to cases where one type of atom is replaced by the same atom in all instances. Specifically, materials on the form X_6FeY_5, where X is either Ca or Mg and Y is either N or P, will be investigated in this study.

It is worth noting that since intermediate bands have the Fermi energy within a band, they are strictly speaking metals, and thus there is no band gap in the usual sense; however, when talking about intermediate bands we refer to the bands above and below it as the conduction and valence bands respectively. We also consider the energy gaps between any of these as meaningful band gaps.

2 Density Functional Theory

Density Functional Theory (DFT) is a method for solving the many-body Schrödinger equation numerically that is based on the theorems by Hohenberg and Khon in 1964 [5], and the equations derived by Kohn and Sham in the following year [7]. In the 1990s it became a more widespread method for quantum chemistry due to increased accuracy [6]. The content in this section is based on the book by Sholl and Steckel [10] unless specified otherwise.

2.1 The Kohn-Sham Equations

The Hohenberg-Kohn theorems read as follows: "The ground-state energy from Schrödinger's equation is a unique functional of the electron density". Followed by: "The electron density that minimizes the energy of the overall functional is the true electron density corresponding to the full solution of the Schrödinger equation". This means that the variational principle can be used to determine the ground-state energy using the energy functional. Using the Born-Oppenheimer approximation the energy functional is

$$E[\psi_i] = -\frac{\hbar^2}{2m}\sum_i \int \psi_i^* \nabla^2 \psi_i d^3r + \int V(\boldsymbol{r}) n(\boldsymbol{r}) d^3r + \frac{e^2}{2}\int\int \frac{n(\boldsymbol{r})n(\boldsymbol{r'})}{|\boldsymbol{r}-\boldsymbol{r'}|} d^3r d^3r' + E_{ion} + E_{XC}[n], \quad (1)$$

where the first term is the electron kinetic energy and the second, third and fourth terms are the Coulomb interactions between pairs of electron-nuclei, electron-electron, and nuclei-nuclei respectively. The fifth and final term, $E_{XC}[n]$, accounts for the non-Coulomb interactions and is the only unknown term; determining this is the key to the Kohn-Sham equations. The Kohn-Sham equations are the set of equations given by

$$\left[-\frac{\hbar^2}{2m}\nabla^2 + V(\boldsymbol{r}) + V_H(\boldsymbol{r}) + V_{XC}(\boldsymbol{r})\right]\psi_i(\boldsymbol{r}) = \varepsilon_i \psi_i(\boldsymbol{r}), \quad (2)$$

which has a similar form to the many-body Shcrödinger equation; however, there is only a single electron and thus no summation over electrons. The role of the potential is represented by an effective potential, $V_{eff}(\boldsymbol{r}) = V(\boldsymbol{r}) + V_H(\boldsymbol{r}) + V_{XC}(\boldsymbol{r})$. The exchange-correlation functional is then defined as

$$V_{XC}(\boldsymbol{r}) = \frac{\delta E_{XC}[n]}{\delta n(\boldsymbol{r})}. \tag{3}$$

2.2 Exchange-Correlation Functionals

The exchange-correlation functional has not been identified in general, only for the trivial system of uniform electron gas. One of the most basic approximations of the functional, the Local Density Approximation (LDA), uses this to set the value of the functional at any given point in space to the corresponding uniform gas solution of the given electron density, so that $V_{XC}^{LDA} = V_{XC}^{gas}[n(\boldsymbol{r})]$.

A more sophisticated, but also more computationally intensive, approximation is the General Gradient Approximation (GGA), which also incorporates the local gradient of the electron density, so all GGA functionals are on the form $V_{XC}^{GGA} = V_{XC}[n(\boldsymbol{r}), \nabla n(\boldsymbol{r})]$. There is no single GGA functional that is optimal for all systems; some rely on empirical parameters that can be modified to fit each specific system better, while others — like the Perdew-Burke-Ernzerhof (PBE) functionals — aim to be a more general-purpose functional only based on theory.

2.3 The Absorption Coefficient

The absorption coefficient is relevant for the analysis of optical properties. The derivation here of how to express it in terms of the energy and the relative dielectric function is largely based on the book by Jasprit Singh [11, p. 349]. The general solution of wave propagation with dissipation can be given on the form

$$\mathbf{E} = \mathbf{E}_0 e^{i(\mathbf{k}\cdot\mathbf{r} - \omega t)}, \tag{4}$$

which when inserted into the Maxwell equation for an electric field in

a medium, reduces it to

$$k^2 = \varepsilon\mu_0\omega^2 + i\sigma\mu_0\omega. \tag{5}$$

This expressed in terms of the speed of light, c, becomes

$$k = \frac{\omega}{c}\sqrt{\varepsilon_r + \frac{i\sigma}{\varepsilon_0\omega}}, \tag{6}$$

where ε_r is the relative dielectric function and the root as a whole can be interpreted as the complex refractive index, n. By separating the refractive index into real and imaginary parts, n_R and n_I, we can then write the equation as

$$k = \frac{n_R\omega}{c} + i\frac{n_I\omega}{c}. \tag{7}$$

Inserting this into equation (4) for propagation in the z-direction results in

$$\mathbf{E} = \mathbf{E}_0 \exp\left(i\omega\left(\frac{n_R z}{c} - t\right)\right)\exp\left(\frac{-n_I\omega z}{c}\right). \tag{8}$$

Here the real-valued exponential is the dampening effect of primary interest to us. The absorption coefficient, α, is identified from the square of this real-valued term:

$$\alpha(\omega) = \frac{2n_I\omega}{c}. \tag{9}$$

Using equation (6) we can also separate the relative dielectric function into real and imaginary parts, ε_R (not to be confused with ε_r) and ε_I, by

$$\begin{aligned} \varepsilon_R &= n_R^2 - n_I^2, \\ \varepsilon_I &= 2n_R n_I. \end{aligned} \tag{10}$$

By solving these for n_I, inserting them into equation (9), and replacing the angular frequency with the corresponding photon energy, we get

$$\alpha(E) = \frac{2E}{\hbar c}\sqrt{\frac{-\varepsilon_R + \sqrt{\varepsilon_R^2 + \varepsilon_I^2}}{2}}. \tag{11}$$

In a previous step, propagation in the z-direction was assumed, but we want a description of all directions, so we use the dielectric tensor, which for hexagonal symmetry is on the form

$$\boldsymbol{\varepsilon_r} = \begin{bmatrix} \varepsilon_\parallel & 0 & 0 \\ 0 & \varepsilon_\parallel & 0 \\ 0 & 0 & \varepsilon_\perp \end{bmatrix}, \tag{12}$$

where $\varepsilon_\parallel$ is the dielectric function parallel to the hexagonal plane and $\varepsilon_\perp$ is the dielectric function orthogonal to the hexagonal plane. Separating it into real and imaginary parts will give matrices on the same form. Since the matrices are diagonal we can separate equation (11) into

$$\begin{aligned} \alpha_\parallel(E) &= \frac{2E}{\hbar c}\sqrt{\frac{-\varepsilon_{R\parallel} + \sqrt{\varepsilon_{R\parallel}^2 + \varepsilon_{I\parallel}^2}}{2}}, \\ \alpha_\perp(E) &= \frac{2E}{\hbar c}\sqrt{\frac{-\varepsilon_{R\perp} + \sqrt{\varepsilon_{R\perp}^2 + \varepsilon_{I\perp}^2}}{2}}, \end{aligned} \tag{13}$$

where $\alpha_\parallel(E)$ and $\alpha_\perp(E)$ are the absorption coefficients for the parallel and orthogonal directions respectively.

3 Computational Method

For the computational calculations, the open-source software Quantum ESPRESSO (QE) [3] was used with pseudopotentials by D. R. Hamann [4]. All the QE calculations were done using Idun, a high-performance computing infrastructure at NTNU [12] and Hemmer, a different HPC infrastructure at NTNU. Simple post-processing and plotting was done in Python using my personal computer.

The first step was to use the QE function *pw.x* to get the relaxed structures of the materials using the variable-cell relax (vc-relax) mode. This calculation involves several energy-minimzations in an iterative process where the atoms are moved after each step based on the result of the step. This is repeated until the energy change is within the given threshold. As input coordinates, the relaxed coordinates given by the AFLOW database entry for Ca_6FeN_5 were used [1]. Note that this unit cell is doubled ($Ca_{12}Fe_2N_{10}$) since the unit cell consists of alternating symmetries of Ca_6FeN_5. For the other variants, the same start coordinates were used, but with the corresponding atoms instead, as they had no corresponding entries in the database. The kinetic energy cutoff parameters, ecutwfc and ecutrho, were set to 125 Ry and 1000 Ry respectively. The number of bands was set to 240, and the starting magnetization was set to 0.6 for the iron atoms. The convergence threshold was set to 10^{-6}. The k-points were set to a uniform grid of size $6 \times 6 \times 3$. The last axis was set to have fewer points because the unit cell is longer in that direction and k-points are in reciprocal space. The resulting coordinates from these calculations were used as input coordinates for all future calculations.

For getting the band structure, the *pw.x* function was used once again, but with the "scf" and "bands" modes. The scf mode does the same energy-minimization as in the vc-relax mode, but rather than iterating over different atomic positions, it simply calculates the properties of the given input coordinates. This is necessary, as the "bands" mode uses the resulting data to extract the band structure data. The settings for these are mostly the same as the previous calculation; however, the convergence threshold was reduced to 10^{-7} for higher accuracy, and the k-point sampling was changed from a uniform grid to following a path through high-symmetry points in the structure. This path was chosen based on the path used by AFLOW [1]. Finally, the QE library's dedicated post-processing function *bands.x* was used

to export this data to a data file that was used to plot the data in Python.

The absorption coefficient does not have a dedicated QE function, but the *epsilon.x* post-processing function has a mode for calculating the dielectric tensor, which can be used in equation (11). This function also requires an energy-minimization to be done prior with *pw.x*, and for this, the settings were as described for the vc-relax calculations. Equation (11) was then implemented using a Python script, which then also plotted the resulting data.

4 Results and Discussion

4.1 Structure of the materials

The vc-relax resulted in essentially the same relative positions of the atoms in the unit cell for all the materials, and also matched the database entry for Ca_6FeN_5 [1]. The main difference between the structures were the bond lengths and the size of the unit cell. The planar FeN bond lengths were 1.80 Å and 1.78 Å for Ca_6FeN_5 and Mg_6FeN_5 respectively, and the planar FeP bond lengths were 2.17 Å and 2.11 Å for Ca_6FeP_5 and Mg_6FeP_5 respectively. A comparison of the unit cell dimensions can be seen in table 1.

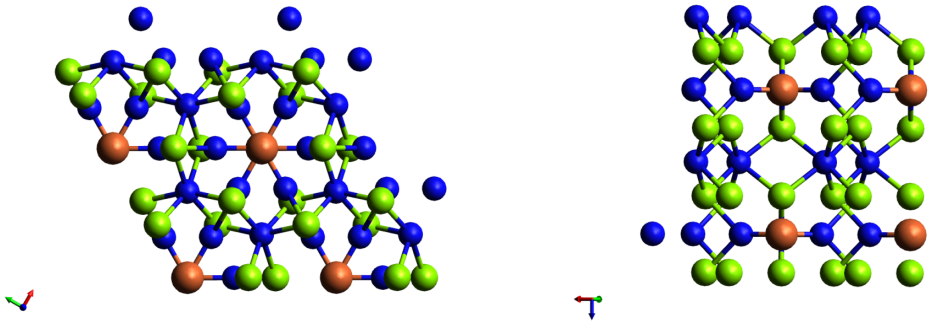

Figure 1: Structure of Ca_6FeN_5 seen in the xy-plane and xz-plane on the left and right respectively. The green atoms are Ca, the red atoms are Fe, and the blue atoms are N. The structure is essentially the same for all four combinations, so the green and blue atoms may also represent Mg and P respectively; although with different bond lengths. See table 1 below.

Table 1: Relaxed lattice parameters of the X_6FeY_5 crystals.

Crystal (X_6FeY_5)	a [Å]	b [Å]	c [Å]	α	β	γ
Ca_6FeN_5	6.24	6.24	12.25	90.0°	90.0°	120.0°
Mg_6FeN_5	5.65	5.65	10.93	90.0°	90.0°	120.0°
Ca_6FeP_5	7.18	7.18	14.30	90.0°	90.0°	120.0°
Mg_6FeP_5	6.48	6.48	13.06	90.0°	90.0°	120.0°

It can be seen that the bond lengths and size of the unit cells increase when substituting with larger atoms, e.g. going from N to P, and decrease when substituting with smaller atoms, as you would expect.

4.2 Band Gap Analysis

For the band gap analysis, we are only interested in transition energies up to about 3 eV, as anything beyond that is of little use in solar cell applications. When analyzing these results it is also important to keep in mind that DFT is known to severely underestimate band gaps, so all apparent bands gaps will likely be larger in reality [9]; however, since the aim of this thesis is to compare band gaps with each other, knowing the exact band gaps is not vital; only the relative sizes of them.

4.2.1 Ca_6FeN_5

For Ca_6FeN_5 there is a clear intermediate band (see figure 2) and the Fermi energy is in the middle of the intermediate band. The valence band starts at about -1 eV, while the conduction band can be interpreted as split into two components: a lower one between 0.5 eV and 1.5 eV, and a higher starting at 2 eV. It is also possible to consider the "lower conduction band" as a second unoccupied intermediate band. The distinction between these two interpretations is not important for the analysis, as it is mostly semantic.

Possible transitions here include transitions from the valence band to the intermediate band at 1.1 eV and upwards. From the intermediate band to the lower conduction band there are some transitions between 0.6 and 1.5 eV, and to the higher one at 2 eV and upwards. There are also possible transitions directly from the valence band to the conduction band starting at 2 eV, but mostly 3 eV and upwards.

In the plot of the absorption coefficients the most interesting peaks are at 0.6 eV, 1.1 eV, and 2.2 eV, which reasonably match the transition energies mentioned above. Comparing with the solar spectrum it is clear that the most significant peak is the one at 2.2 eV, as it is close to the optimal wavelength, while the peaks at 0.6 eV and 1.1 eV are far-off; however, taking into account band gap underestimation, the peaks may in reality be at significantly higher energies than they appear here, and thus be more useful in the context of a solar cell. The peak at 2.2 eV would likely still be useful if the peak was shifted to higher energies, but not as much as it appears here.

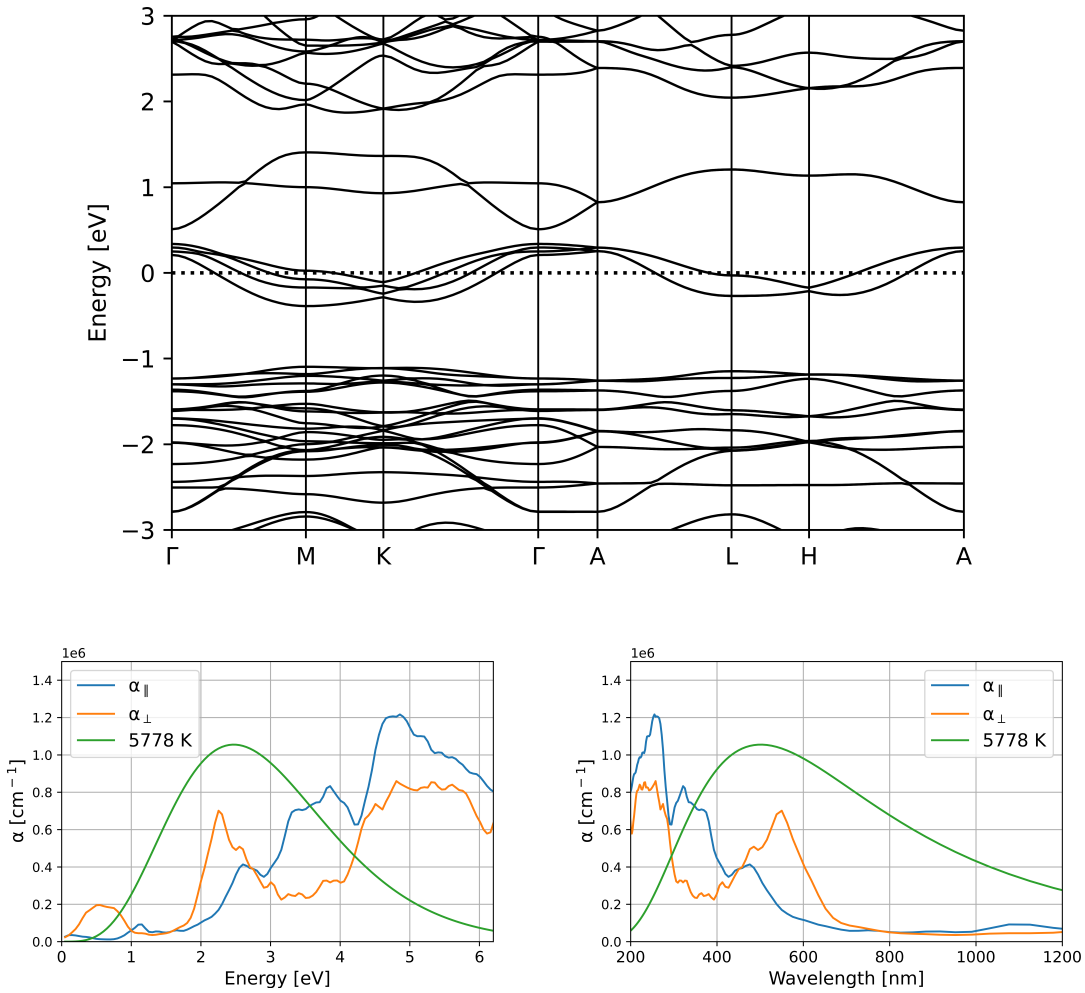

Figure 2: Results for Ca_6FeN_5. **Top:** The electronic band structure. Along the horizontal axis we have paths through the high-symmetry points in k-space. Along the vertical axis we have the energies, where 0 is the Fermi energy, marked with a dotted line. **Bottom left:** The blue and orange graphs are the absorption coefficients for the parallel and orthogonal directions respectively as a function of photon energy. The green graph represents the solar spectrum in arbitrary units. **Bottom right:** The same absorption coefficients and solar spectrum as functions of wavelength.

Overall Ca_6FeN_5 meets the basic criteria of a useful intermediate band as already shown by Baquião and Dalpian [2] and also matches well with AFLOW [1]. This means it is a good baseline for comparison with the other variants as expected.

4.2.2 Mg_6FeN_5

For Mg_6FeN_5 there is also a clear intermediate band (see figure 3); however, the lower section of the conduction band appears to have "merged" with the intermediate band as compared to Ca_6FeN_5. This means that the Fermi energy is no longer in the middle of the intermediate band and supports the idea that considering the band in Ca_6FeN_5 a second intermediate band is reasonable. The width of the intermediate band also increases drastically to over 2 eV. The rest of the conduction band has also been pushed up substantially from 2 eV to a bit under 3 eV, while the valence band has only been pushed down slightly.

From the valence band to the intermediate band there are possible transitions at 1.3 eV and upwards. The gap between the occupied part of the intermediate band and the conduction band is too large to produce any transition energies in our range of interest, especially when you account for DFT underestimation of band gaps. Obviously, the same applies for transitions directly from the valence band to the conduction band.

In the plot of the absorption coefficients the most interesting peaks are at 0.3 eV, 1.3 eV, and 3.4 eV. The one at 0.3 eV must be from intraband transitions in the intermediate band. The peak at 1.3 eV corresponds well with the gap from the valence band to the intermediate band, but can also include more intraband transitions. The peak at 3.4 eV is comparable to the 2.2 eV peak in figure 2 and likely reflects the increased gap between the intermediate band and the conduction band.

The substitution from Ca to Mg led to larger band gaps as well as a wider intermediate band, both of which are undesirable changes in this case, especially the widening of the intermediate band.

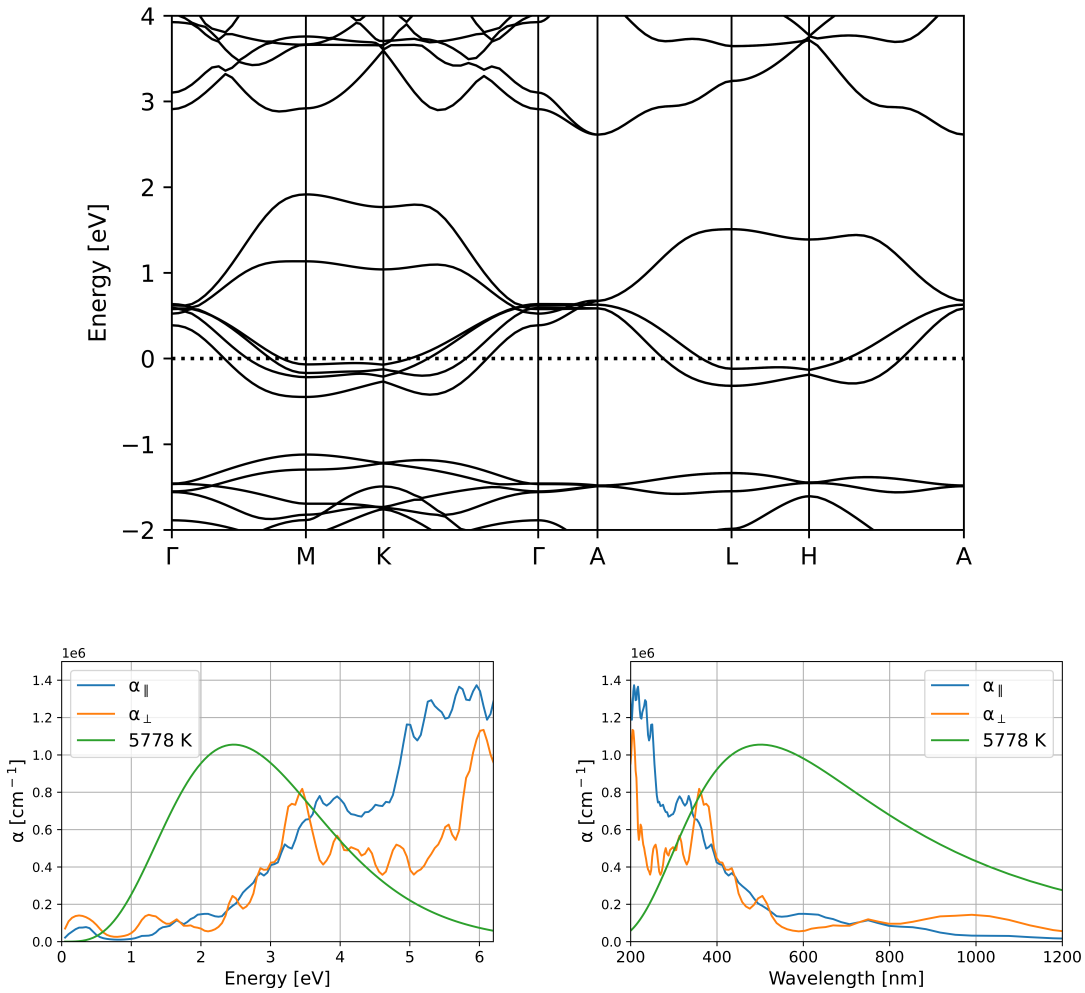

Figure 3: Results for Mg_6FeN_5. **Top:** The electronic band structure. Along the horizontal axis we have paths through the high-symmetry points in k-space. Along the vertical axis we have the energies, where 0 is the Fermi energy, marked with a dotted line. **Bottom left:** The blue and orange graphs are the absorption coefficients for the parallel and orthogonal directions respectively as a function of photon energy. The green graph represents the solar spectrum in arbitrary units. **Bottom right:** The same absorption coefficients and solar spectrum as functions of wavelength.

4.2.3 Ca_6FeP_5

For Ca_6FeP_5 the intermediate band is very close to the valence band and its status as an intermediate band is therefore questionable (see figure 4). The "lower conduction band" is more clearly separated from the intermediate band and is much closer to the rest of the conduction band compared to Ca_6FeN_5. It has also pulled the rest of the conduction band closer to the intermediate band, but not drastically so. Qualitatively this is the opposite of what happened for Mg_6FeN_5.

Because the separation between the valence band and the intermediate band is practically non-existent, it is not as meaningful to talk about transition energies between them. From the intermediate band to the conduction band, which is the only real band gap left, there are transition energies that likely correspond to the peaks at 1.4 eV and 2.1 eV in the absorption coefficient plot.

The substitution from N to P practically led to a loss of the intermediate band due to the distance to the valence band becoming negligible.

4.2.4 Mg_6FeP_5

For Mg_6FeP_5 both the band gaps are practically gone and the remnant of the intermediate band is barely recognizable, so the material is undeniably a metal. Because of this, the absorption coefficient plots are not of great interest either.

4.2.5 Comparisons

It was known beforehand that Ca_6FeN_5 already has desirable properties, so it is of no surprise that the other variants are less ideal. Above the substitutions were described as being done from Ca_6FeN_5 to the other variants, but of course the direction of change is arbitrary; by considering them in the opposite direction, they can be thought of as successful substitutions that led to more desirable properties. It is reasonable to assume a person analyzing the band structure of Mg_6FeN_5 or Ca_6FeP_5 without any foreknowledge of Ca_6FeN_5 would be able to identify them as at least somewhat close to being intermediate bands with desirable properties for solar cells.

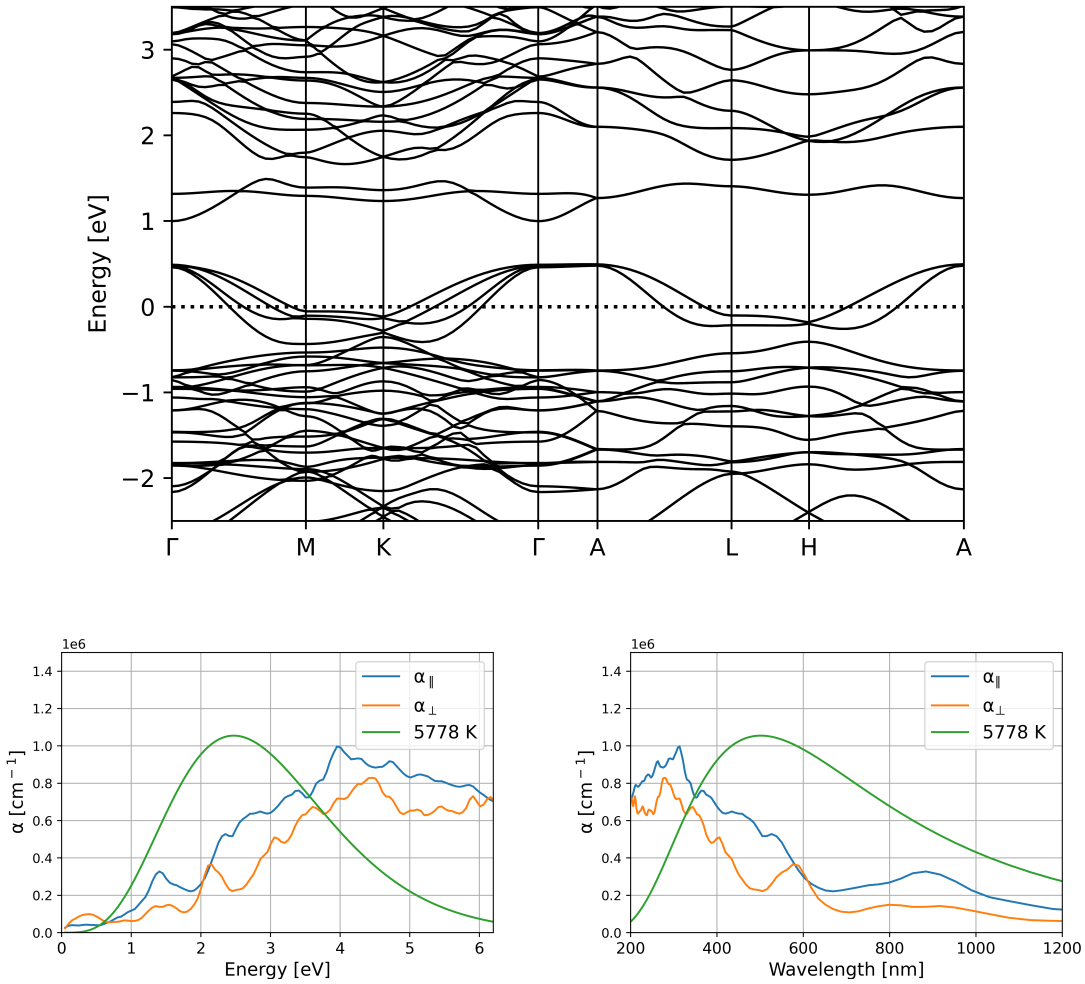

Figure 4: Results for Ca_6FeP_5. **Top:** The electronic band structure. Along the horizontal axis we have paths through the high-symmetry points in k-space. Along the vertical axis we have the energies, where 0 is the Fermi energy, marked with a dotted line. **Bottom left:** The blue and orange graphs are the absorption coefficients for the parallel and orthogonal directions respectively as a function of photon energy. The green graph represents the solar spectrum in arbitrary units. **Bottom right:** The same absorption coefficients and solar spectrum as functions of wavelength.

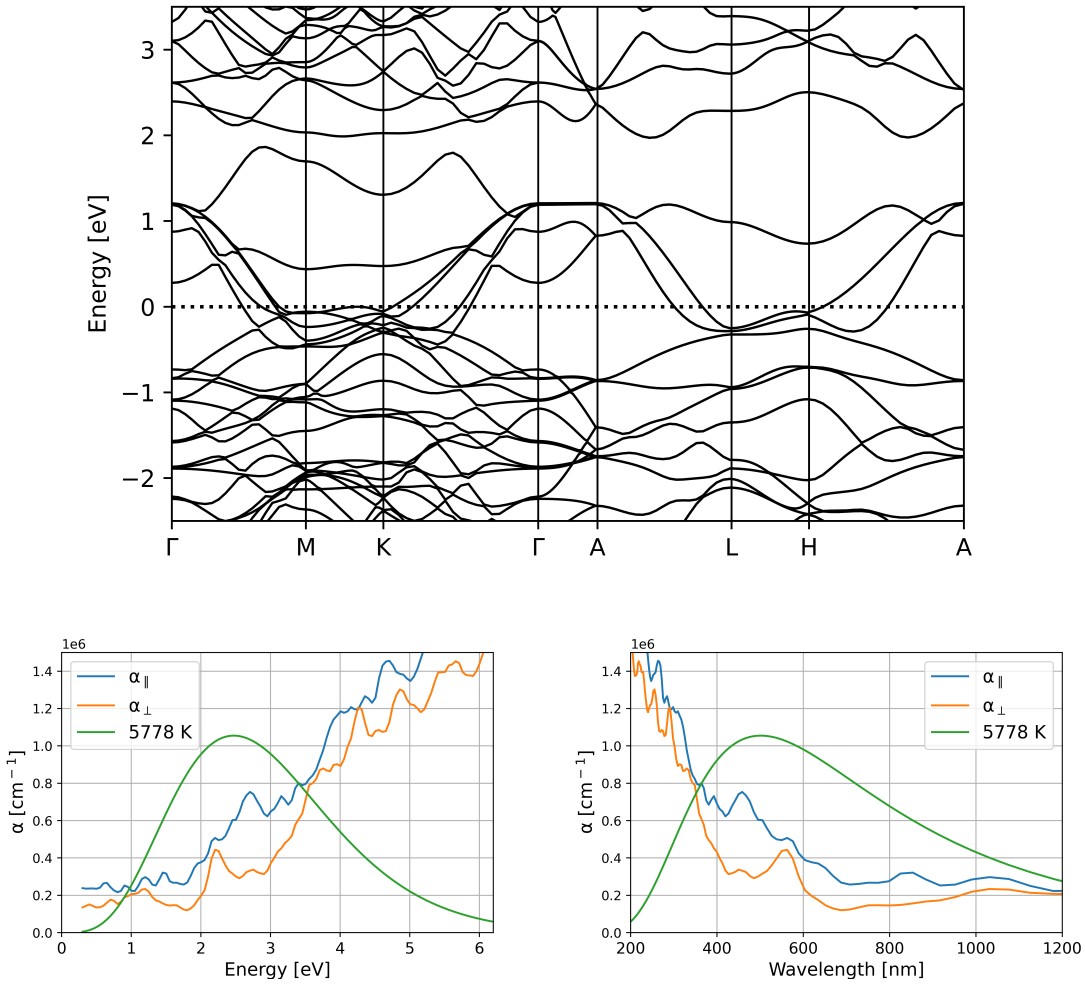

Figure 5: Results for Mg_6FeP_5. **Top:** The electronic band structure. Along the horizontal axis we have paths through the high-symmetry points in k-space. Along the vertical axis we have the energies, where 0 is the Fermi energy, marked with a dotted line. **Bottom left:** The blue and orange graphs are the absorption coefficients for the parallel and orthogonal directions respectively as a function of photon energy. The green graph represents the solar spectrum in arbitrary units. **Bottom right:** The same absorption coefficients and solar spectrum as functions of wavelength.

They could then "discover" Ca_6FeN_5 by following a process like the one described in this study. Although, the same can not necessarily be said of Mg_6FeP_5.

The band structures of Mg_6FeN_5 and Ca_6FeP_5 deviating from the one of Ca_6FeN_5 in qualitatively opposite ways is particularly interesting. As seen in table 1, they also deviate in qualitatively opposite ways in terms of dimensions, both in terms of the size of the unit cell and the bond lengths. With such a small sample size it can not necessarily be concluded that these are related, but it may suggest that there is a pattern to be found. That way, rather than doing substitutions at random, one can make more targeted alterations for specific changes one might want to produce, like increasing or decreasing the size of the band gaps.

In the case of Mg_6FeP_5 it is interesting to note that even something that doesn't look particularly promising as a candidate could be only two simple modifications away from being something with desirable properties; however, that does not necessarily mean checking every possible material is an efficient use of resources in general.

4.3 Further Studies

There are many options for further studies. The most obvious example is to do equivalent studies for different structures, like starting with materials that have structures reminiscent of intermediate bands with the goal of finding a material with an intermediate band suitable for solar cells. Another option, although maybe not as practically viable, is to do substitutions to even heavier atoms as well.

As mentioned in the introduction, looking at partial substitutions would also be of interest. Rather than only choosing between Ca or Mg and N or P, there could be a whole array of options: $Ca_xMg_{(6-x)}FeN_yP_{(5-y)}$, where x and y are integers. For this one would have to be mindful of all the different ways one could choose to substitute a single atom, as they might not give the same end result. It would be interesting to see if this only led to band structures that are part-way between the ones seen here or if the potentially unbalanced structures would cause other changes.

Fe could also be subject to substitutions and is not necessarily limited

to the same group, as other transition metals could give the same formal charge. Other atoms do not necessarily need to be restricted to the same group either, as long as the total formal charge remains the same. For example, one could start with Al_2O_3, upscale it to a basis of Al_8O_{12}, and then replace some Al with Si while replacing the same number of O with N to compensate. This gives a range of options $Al_{(8-x)}Si_xN_xO_{(12-x)}$, where x is an integer.

5 Conclusion

Previous results for the electronic band structure of Ca_6FeN_5 have been verified and new results for Mg_6FeN_5, Ca_6FeP_5, and Mg_6FeP_5 have been presented, as well as a calculation of the absorption coefficient for all variants. Mg_6FeN_5 could be considered to have an intermediate band, but with a lower level of occupancy and a much wider band than ideal. Ca_6FeP_5 does not have an intermediate band as the gap to the valence band is negligible, but it is not far from being one. Mg_6FeP_5 does not have a structure that is reasonably recognizable as close to being an intermediate band.

This study does not present any new materials of interest, but instead demonstrates a method for identifying new materials using DFT by modifying known structures. It has shown that substituting atoms with other atoms can have a significant effect on the electronic band structure, including increasing or decreasing the size of the band gaps, while keeping the overall electronic band structure comparable and recognizable in most cases.

References

[1] *AFLOW Ca6FeN5*. URL: https://aflow.org/material/?id=aflow:aaa02a361ad49a25.

[2] Douglas J.R. Baquião and Gustavo M. Dalpian. 'Computational screening of bulk materials with intrinsic intermediate band'. In: *Computational Materials Science* 158 (2019), pp. 382–388. ISSN: 0927-0256. DOI: https://doi.org/10.1016/j.commatsci.2018.11.030. URL: https://www.sciencedirect.com/science/article/pii/S0927025618307572.

[3] Paolo Giannozzi et al. 'QUANTUM ESPRESSO: a modular and open-source software project for quantum simulations of materials'. In: *Journal of Physics: Condensed Matter* 21.39 (Sept. 2009), p. 395502. DOI: 10.1088/0953-8984/21/39/395502. URL: https://dx.doi.org/10.1088/0953-8984/21/39/395502.

[4] D. R. Hamann. 'Optimized norm-conserving Vanderbilt pseudopotentials'. In: *Phys. Rev. B* 88 (8 Aug. 2013), p. 085117. DOI: 10.1103/PhysRevB.88.085117. URL: https://link.aps.org/doi/10.1103/PhysRevB.88.085117.

[5] P. Hohenberg and W. Kohn. 'Inhomogeneous Electron Gas'. In: *Phys. Rev.* 136 (3B Nov. 1964), B864–B871. DOI: 10.1103/PhysRev.136.B864. URL: https://link.aps.org/doi/10.1103/PhysRev.136.B864.

[6] R. O. Jones. 'Density functional theory: Its origins, rise to prominence, and future'. In: *Rev. Mod. Phys.* 87 (3 Aug. 2015), pp. 897–923. DOI: 10.1103/RevModPhys.87.897. URL: https://link.aps.org/doi/10.1103/RevModPhys.87.897.

[7] W. Kohn and L. J. Sham. 'Self-Consistent Equations Including Exchange and Correlation Effects'. In: *Phys. Rev.* 140 (4A Nov. 1965), A1133–A1138. DOI: 10.1103/PhysRev.140.A1133. URL: https://link.aps.org/doi/10.1103/PhysRev.140.A1133.

[8] Antonio Luque and Antonio Martı. 'Increasing the Efficiency of Ideal Solar Cells by Photon Induced Transitions at Intermediate Levels'. In: *Phys. Rev. Lett.* 78 (26 June 1997), pp. 5014–5017. DOI: 10.1103/PhysRevLett.78.5014. URL: https://link.aps.org/doi/10.1103/PhysRevLett.78.5014.

[9] John P. Perdew and Mel Levy. 'Physical Content of the Exact Kohn-Sham Orbital Energies: Band Gaps and Derivative Discontinuities'. In: *Phys. Rev. Lett.* 51 (20 Nov. 1983), pp. 1884–1887. DOI: 10.1103/PhysRevLett.51.1884. URL: https://link.aps.org/doi/10.1103/PhysRevLett.51.1884.

[10] D. S. Sholl and J. A. Steckel. *Density Functional Theory: A Practical Introduction*. John Wiley and Sons, Inc., 2009. ISBN: 9780470373170.

[11] Jasprit Singh. *Electronic and Optoelectronic Properties of Semiconductor Structures*. Cambridge University Press, 2003. DOI: 10.1017/CBO9780511805745.

[12] Magnus Själander et al. *EPIC: An Energy-Efficient, High-Performance GPGPU Computing Research Infrastructure*. 2019. arXiv: 1912.05848 [cs.DC].

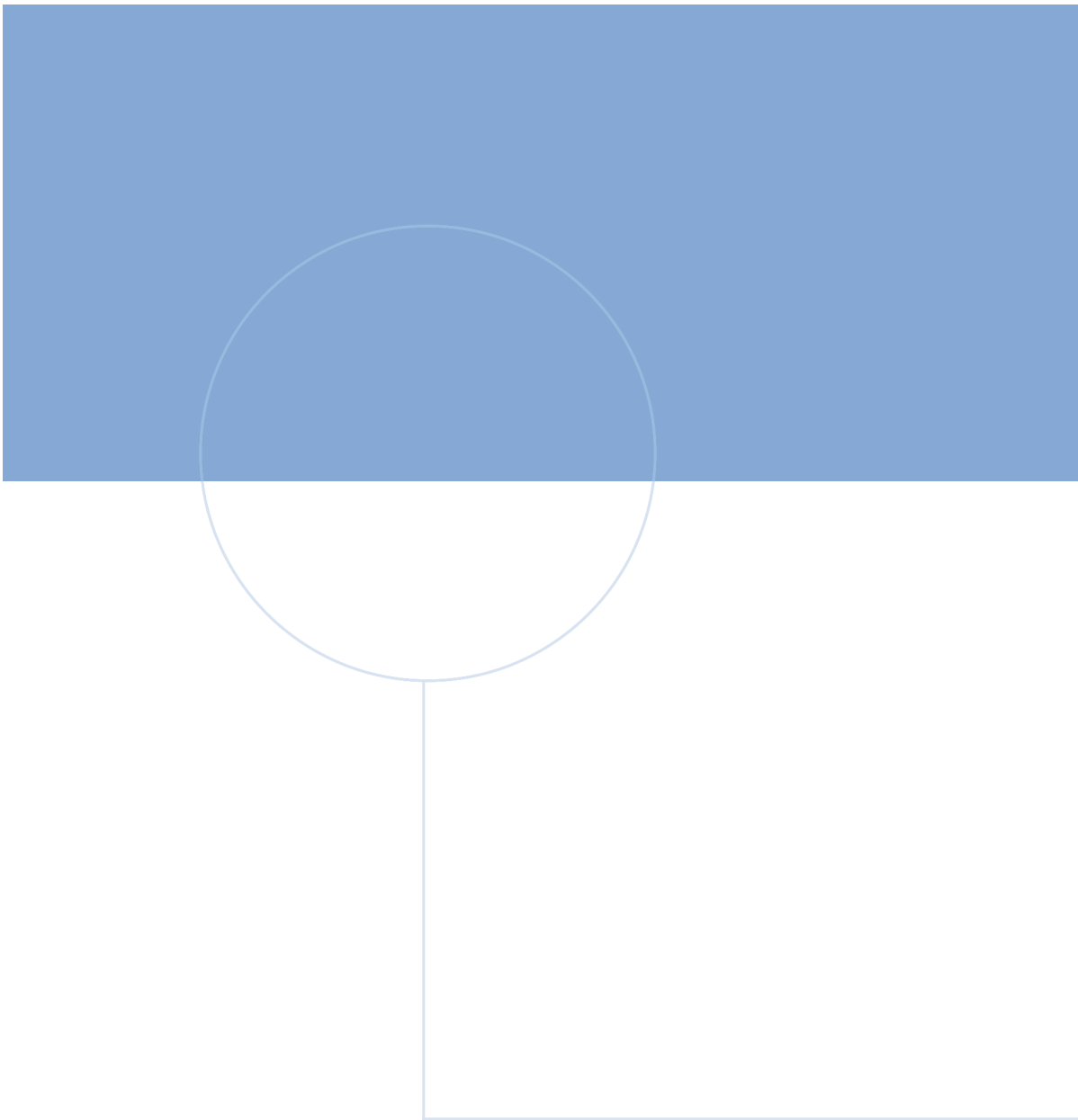

NTNU

Norwegian University of
Science and Technology